2024 IEEE/RSJ International Conference on Intelligent Robots and Systems (IROS)
October 14-18, 2024. Abu Dhabi, UAE

Design and Control of a Soft Supernumerary Robotic Limb Based on Fiber-Reinforced Actuator

Tianyi Zhang, Jiajun Xu, *Member*, *IEEE*, Yonghua Lu, Mengcheng Zhao,
Kaizhen Huang, Bai Chen, Xuyan Hou, Youfu Li, *Fellow, IEEE*

***Abstract*—Supernumerary robotic limbs (SRLs) provide additional wearable limbs to enhance the user's physical abilities. Most SRLs employ rigid structures, resulting in uncomfortable wearing experience and insufficient flexible manipulation. As a new type of SRL, soft SRLs offer operational flexibility, lightweight structure, and wearing safety, compensating for the shortcomings of rigid SRLs. However, due to the complex actuation mechanisms, soft SRLs pose challenges in multiple deformations and accurate controlling. In this paper, a soft SRL actuated by fiber-reinforced actuators (FRAs) is proposed. A kinematic model is established to capture the posture of the SRL. A control system is proposed to adjust the SRL posture precisely by configuration of the FRAs. Finally, the accuracy of the proposed control strategy is verified through experiments, and the SRL prototype exhibits flexibility and adaptability to various scenarios, effectively assisting users in accomplishing complex tasks.**

I. Introduction

As a type of wearable robot, supernumerary robotic limbs (SRLs) significantly extend users' capabilities and assist them in completing tasks by providing extra limbs and mimicking the movements of users [1, 7]. In recent years, SRL has been applied to various aspects of industrial production and daily life. These include serving as an additional arm to hold parts for users during assembly processes [2], providing support to users in a comfortable posture in tasks requiring proximity to the ground [3], carrying items when both hands are occupied [4], and assisting users in tasks such as harvesting and cleaning through remote operation [5, 6]. While the benefits of SRL are evident, current SRL research generally adopts rigid structures with motors or artificial tendons as the driving units, exhibiting heavy weights, low flexibility, and safety risks, which imposes several limitations.

With the deepening research on soft materials, a new type of SRL called soft SRL has been proposed. Soft SRLs can actively modify their structures and stiffness to adapt to complex environments [9]. Their lightweight structures provide greater flexibility, and the compliant driving mechanism makes them safer [8, 1011], representing a potential solution to address the existing issues.

Soft SRLs typically consist of multiple soft actuators whose collective deformations contribute to the overall deformation of the whole SRLs. The current research on soft SRLs includes a biomimetic flipper-like soft finger worn on the user's wrist to assist in grasping operations [12], a soft-poly limb capable of performing various tasks [13], and a fabric-based SRL with high flexibility and load-bearing capacity [14] and so on. Soft actuators primarily comprise materials such as silicone rubber or polyethylene, whose properties exhibit hyper-elastic deformation, contrasting with rigid materials. Furthermore, with the increase in soft actuators, the motion complexity of soft SRL also increases, leading to greater control difficulty. Current research relies mainly on finite element methods or constant curvature methods [25] to estimate soft SRL's posture, which is inefficient and inaccurate. Therefore, finding an effective model to estimate the posture of the soft SRL and designing corresponding control methods for its operation is essential.

In this paper, a soft SRL actuated by FRA is proposed. Inspired by octopus arms, the SRL is composed of multiple parallel FRA segments connected in series, enabling it to perform in various postures. Furthermore, the kinematic model for the SRL is established, along with the control system, to control the SRL posture precisely. Finally, experiments are conducted to verify the SRL's control accuracy, and the motion performance of SRL's prototype is carried out, exhibiting its flexibility and adaptability to various scenarios. The main contributions are as follows:

- An SRL adopting a fiber-reinforced strategy is proposed, which achieves posture changes by varying air pressure.
- A kinematic model for the SRL is established, capable of predicting the state of each FRA within the SRL, and designed a control strategy to accurately achieve complex postures of the SRL.
- Experimentally validated the accuracy of the kinematic model, demonstrating that the SRL can collaborate with users to complete tasks and adapt to various scenarios.

II. Structure Design and Fabrication of the SRL

A. Analysis of Fiber-Reinforced Actuators

Octopuses give great inspiration about the structure of SRL. The muscular tissue of octopus arms consists of three main types of muscle fibers in different orientations. By selectively activating specific muscle fibers, octopus arms can perform a variety of complex movements [15, 16].

This work was supported in part by the National Natural Science Foundation of China under Grant 52205018, in part by the Natural Science Foundation of Jiangsu Province under Grant BK20220894, in part by the State Key Laboratory of Robotics and Systems (HIT) under Grant SKLRS-2023-KF-25, in part by State key Laboratory of Robotics under Grant 2023-O16, and in part by the China Postdoctoral Science Foundation under Grant 2024M754124. (Corresponding author: Jiajun Xu.)

Tianyi Zhang, Jiajun Xu, Yonghua Lu, Mengcheng Zhao, Kaizhen Huang and Bai Chen are with the college of Mechanical and Electrical Engineering, Nanjing University of Aeronautics and Astronautics, Nanjing 210016, China (e-mail: zhangtianyi096@nuaa.edu.cn; xujiajun@nuaa.edu.cn; nuaa_lyh@nuaa.edu.cn; zhaomengcheng@nuaa.edu.cn; huangkaizhen@nuaa.edu.cn; chenbye@nuaa.edu.cn).

Xuyan Hou is with the School of Mechatronics Engineering, Harbin Institute of Technology, Harbin 150001, China (e-mail: houxuyan@hit.edu.cn).

Y. Li is with Department of Mechanical Engineering, City University of Hong Kong, Hong Kong 999077, China (e-mail: meyfli@cityu.edu.hk).

Inspired by the octopus arm, a fiber-reinforced mechanism is employed to mimic the functionality of muscle fibers in octopus arm. Fiber-reinforced actuator (FRA) is a hollow cylindrical silicone body with fibers wound around the skin, as shown in Fig. 1(a). The FRA will undergo deformation when pressurized air is injected into the core. By combining multiple FRAs and inflating them with different air pressures individually, a variety of postures different from those of individual FRAs can be achieved. Therefore, FRA is chosen as the actuator for SRLs to mimic muscles in the octopus arm.

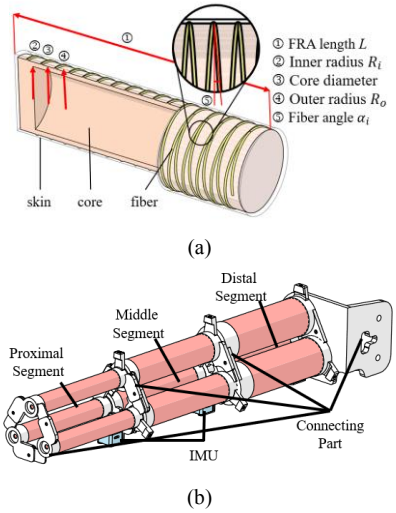

Figure 1. Structure of FRA and SRL. (a) FRA is composed of 3 parts: core fiber and skin, and the structure parameter is shown; (b) SRL's structure design and layout, SRL is composed of multiple segments connected in series, with each segment made up of parallel FRAs of the same radius.

The mechanical properties of hyper-elastic materials are determined using the ASTM D412 standard testing method. The data is then fitted to hyper-elastic models using a nonlinear least squares method to obtain the most accurate material property coefficients [17]. The primary material for SRLs is Dragon Skin 30 (Smooth-On, Inc., Macungie, PA), with a Shore hardness of 30A. Additionally, to enhance the overall stiffness of the SRL, SmoothSil-950 (Smooth-On, Inc., Macungie, PA) with a Shore hardness of 50A is chosen as the outer shell for proximal FRAs.

Hyper-elastic materials require using hyper-elastic models to describe the relationship between strain and stress. Among them, Dragon Skin 30 is better suited for the Yeoh model, while SmoothSil-950 is more suitable for the Neo-Hooke model [18]. By employing the finite element method, a simulation model for FRA can be established through ABAQUS, facilitating preliminary deformation analysis of the FRA. The material of the FRA's elastic body is modeled as tetrahedral quadratic hybrid elements (element type C3D10H), and the fibers use Kevlar material, with Young's modulus E_f of 31,067 MPa and Poisson's ratio λ_f of 0.36, modeled as quadratic beam elements (element type B32) [19, 20]. The coefficients for both materials can be obtained using the method in reference [21]: $c_{10} = 0.0861$, $c_{20} = 0.0136$ for Dragon Skin 30 and $c_{30} = 0.34$ for SmoothSil-950.

B. *Structure Design and Fabrication of SRL*

The structure of SRL, as shown in Fig. 1(b), consists of multiple segments connected in series, each comprising three parallel FRAs. The length of the SRL is comparable to that of a human upper limb to provide better assistance. Applying different pressures to the parallel FRAs enables the SRL to achieve various postures. The SRL's segments employ a gradual reduction in radius design for each parallel segment. Preliminary analysis through finite element method shows that when the reduction *ratio* ($ratio = r_{distal}/r_{proximal}$) is 0.5, both the load-bearing capacity and flexibility of the SRL achieve optimal performance.

The fabrication of the SRL involves several steps below. First, the inner core of the actuator is molded using 3D-printed molds. After assembling the molds, liquid silicone rubber is poured into them and left to solidify for 12 hours until fully cured, completing the production of the inner core, as shown in Fig. 2(a). Second, Kevlar fibers are uniformly wound around the core surface, as shown in Fig. 2(b). Third, a set of larger-sized molds is used to create the outer skin of the FRA, as shown in Fig. 2(c). The outer skin of the proximal FRAs is used SmoothSil-950 to enhance the proximal segment stiffness. In the fourth step, the fabricated FRAs are bonded with the 3D-printed connecting parts in parallel to form parallel segments, as shown in Fig. 2(d). The final step involves using bolts to connect the three parallel segments, thus completing the assembly of the SRL, as shown in Fig. 2(e). The FRA is made of soft material, which is prone to damage, therefore, the connecting parts are designed as modular components. When an FRA is damaged, it can be easily removed for repair or replacement, significantly reducing costs. Sil-Poxy (Smooth-On, Inc.) is used to bond the FRAs to the connecting parts.

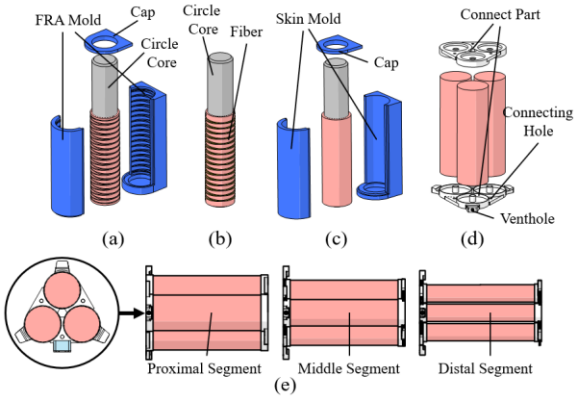

Figure 2. Fabrication processing of the SRL. (a) The fabrication of FRA's core; (b) Kevlar fibers are wrapped around the core surface; (c) The fabrication of FRA's skin; (d) FRA's ends are bonded with connecting parts; (e) Connecting three segments to complete the assembly of the SRL.

III. Modeling of the SRL

A. *Analytic Model of FRA*

The properties of the FRA determine its behavior. The fiber angle and the number of fibers influence the behavior of the FRA. The FRA can be divided into two layers: the isotropic inner layer with silicone rubber and the anisotropic outer layer with fiber wound around silicone rubber, and the deformation between the two layers is continuous.

The FRA has an initial inner radius R_i and outer radius R_o, and the boundary radius between the two layers is R_m, as shown in Fig. 1(a) ①-⑤. The fibers are wound with the angle of α_1, α_2, and the initial orientations are $S_i = [0 \quad cos\alpha_i \quad sin\alpha_i]^T$. Establish a coordinate system for the FRA using cylindrical coordinates, and assuming the coordinates of a point on it is $(R \quad \Theta \quad Z)^T$. When the FRA is pressured, its coordinates become $(r \quad \theta \quad z)^T$ with FRA's length changes from L to l, and the radius change to r_i, r_m, r_0. The deformation gradient F is used to demonstrate the coordinate transformation:

$$F = \begin{bmatrix} \frac{\delta r}{\delta R} & \frac{\delta r}{R\delta\theta} & \frac{\delta r}{\delta Z} \\ \frac{r\delta\theta}{\delta R} & \frac{r\delta\theta}{R\delta\theta} & \frac{r\delta\theta}{\delta Z} \\ \frac{\delta z}{\delta R} & \frac{\delta z}{R\delta\theta} & \frac{\delta z}{\delta Z} \end{bmatrix} = \begin{bmatrix} \frac{1}{\lambda_\theta \lambda_z} & 0 & 0 \\ 0 & \lambda_\theta & r\frac{\phi}{L} \\ 0 & 0 & \lambda_z \end{bmatrix} \quad (1)$$

where $\lambda_z = \frac{z}{Z}$ and $\lambda_\theta = \frac{r}{R}$ denote the axial elongation and the radial expansion, and the circumferential rotation angle is defined as ϕ. The left Cauchy–Green deformation tensor $B = FF^T$, and the tensor invariants $I_m = tr(B)$ are calculated, $I_i = F \cdot S_i \cdot F \cdot S_i$ have the same meaning as I_1, representing the tensor invariants of fibers.

The two layers have different strain energy expressions. Let W^{in}, W^{out} be the strain energy of inner and outer layers. The strain energy of inner layer is $W^{DS30} = \sum_{i=1}^{2} c_{i0}(I_m - 3)^i$ or $W^{950} = c_{30}(I_m - 3)$ for the two materials. For the outer layer, the strain energy of fibers is considered: $W^{out} = c_1 W^{DS30/950} + c_2\left(E_f\left(\sqrt{I_i} - 1\right)^2/2\right)$, where $c_1 = V_{sil} / \left(V_{sil} + V_{fiber}\right)$ and $c_2 = V_{fiber} / \left(V_{sil} + V_{fiber}\right)$ are the volume ratio of silicone materials and fibers in the outer layer, E_f represents Young's modulus of fibers.

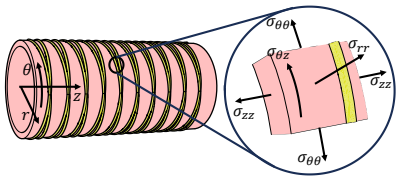

Figure 3. Stress distribution of FRA microelements.

The strain energy equations can be used to calculate the Cauchy stress:

$$\sigma^{in} = \begin{bmatrix} \sigma_{rr}^{in} & \sigma_{r\theta}^{in} & \sigma_{rz}^{in} \\ \sigma_{\theta r}^{in} & \sigma_{\theta\theta}^{in} & \sigma_{\theta z}^{in} \\ \sigma_{zr}^{in} & \sigma_{z\theta}^{in} & \sigma_{zz}^{in} \end{bmatrix} = 2W_1^{in}B - pI$$

$$\sigma^{out} = 2W_1^{out}B + 2W_4^{out}s_1 \otimes s_1 + 2W_6^{out}s_2 \otimes s_2 - pI \quad (2)$$

where $W_i = \frac{\delta W}{\delta I_i}$. p represents the hydrostatic pressure in the material which must be removed [24], and I is the identity matrix. $\otimes$ represents the Kronecker's product operation of the matrix ($A \otimes B = \begin{bmatrix} a_{11}B & \cdots & a_{1n}B \\ \vdots & \ddots & \vdots \\ a_{m1}B & \cdots & a_{mn}B \end{bmatrix}$). An element of the FRA and associated stress are shown in Fig. 3. The relationship between the inner pressure P_F and the deformed FRA radius is shown:

$$P_F = \int_{r_i}^{r_m} \frac{\sigma_{\theta\theta}^{in} - \sigma_{rr}^{in}}{r} dr + \int_{r_m}^{r_o} \frac{\sigma_{\theta\theta}^{out} - \sigma_{rr}^{out}}{r} dr \quad (3)$$

By calculating (3), λ_z as a function of P_F can be obtained. The FRA is equipped with symmetric dual fibers, limiting its radial expansion and torsion ($\lambda_\theta, \phi \approx 0$).

B. Kinematic Model of the Parallel Segment

In this section, the modeling for parallel segments is extended based on the Cosserat rod theory, which represents a linear object as a set of continuous points. When using the theory, it is assumed that the radial deformation generated by the linear model is approximated to be zero, which is similar to the deformation characteristics of the FRA introduced in the section above, leading to the neutral axis and the center axis approximately coincide.

The position of the FRA in a segment is defined by its neutral axis $p_i(s_i)$, which is a function of length. $s_i \in [0 \quad l_i]$ represents the points on the neutral axis of the *i*-th FRA, and $R_i(s_i)$ represents the orientation of the cross-section on the neutral axis of the FRA in the form of an orthonormal matrix. Assuming that the neutral axis of is along the z-axis direction, two vectors, then $u_i(s_i) = [u_1 \quad u_2 \quad u_3]^T$ and $v_i(s_i) = [v_1 \quad v_2 \quad v_3]^T$ are defined. u_1 and u_2 represent the level of bending in two orientations perpendicular to each other within the cross-section along the neutral axis, while u_3 represents torsion perpendicular to the cross-section. v_1 and v_2 represent shearing and v_3 represents elongation. The change of bending and elongation of the neutral axis in the local coordinate system of a FRA is demonstrated as:

$$\frac{dp_i(s_i)}{ds_i} = R_i(s_i)v_i(s_i), \frac{dR_i(s_i)}{ds_i} = R_i(s_i)\hat{u}_i(s_i) \quad (4)$$

where $\hat{u}_i$ denotes as $\hat{u}_i = \begin{bmatrix} 0 & -u_3 & u_2 \\ u_3 & 0 & -u_1 \\ -u_2 & u_1 & 0 \end{bmatrix}$. If the initial coordinates $p_i(0)$ and $R_i(0)$, along with $u_i(s_i)$ and $v_i(s_i)$ are known, the coordinates of the neutral axis can be obtained. Therefore, additional solving for $u_i(s_i)$ and $v_i(s_i)$ are performed.

The deformation of the neutral axis be influenced by internal forces $n_i(s_i) = [n_{ix} \quad n_{iy} \quad n_{iz}]^T$ and moments $m_i(s_i) = [m_{ix} \quad m_{iy} \quad m_{iz}]^T$ as well. By using the differential equations of static equilibrium for a Cosserat rod, the trends of change of both $n_i(s_i)$ and $m_i(s_i)$ can be expressed as follows:

$$\frac{dn_i(s_i)}{ds_i} = -f_i(s_i), \frac{dm_i(s_i)}{ds_i} = -\frac{dp_i(s_i)}{ds_i} \times n_i(s_i) - l_i(s_i) \quad (5)$$

where $f_i(s_i)$ and $l_i(s_i)$ are external forces and moments distribute on the FRA, containing gravity and interaction loads, as shown in Fig. 4.

The shearing (s) and elongation (e) in local system of the point s_i are related to the forces and stiffness $K_{se} = \mathrm{diag}(GA \quad GA \quad EA)$. Similarly, bending (b) and twisting (t) strains are related to moments and the stiffness $K_{bt} = \mathrm{diag}(EI_x \quad EI_y \quad GI_z)$. E, G represent elastic modulus and shear modulus [22]. $A = \pi(R_o^2 - R_i^2)$ represents the area of the cross-section. $I_x = I_y = \frac{\pi(R_0^4 - R_i^4)}{4}$ are the second area moment about the local x- and y-axis direction. $I_z = I_x + I_y$ is the polar area moment about the local z-axis direction. According to the laws of elasticity, appropriate constitutive relationships can be established between $n_i(s_i)$, $m_i(s_i)$, $u_i(s_i)$, and $v_i(s_i)$ through dynamic equations:

$$n_i(s_i) = R_i(s_i)K_{se}(v_i(s_i) - v_i^*)$$

$$m_i(s_i) = R_i(s_i)K_{bt}(u_i(s_i) - u_i^*) \quad (6)$$

where u_i^* and v_i^* are initial configurations. Since the above assumption is that the neutral axis is along the z-axes, $u_i^* = [0 \quad 0 \quad 0]^T$, $v_i^* = [0 \quad 0 \quad 1]^T$ are applied for calculation. Thus, a differential equations system describing $p_i(s_i)$, $R_i(s_i)$, $n_i(s_i)$ and $m_i(s_i)$ is obtained by integrate (4) - (6).

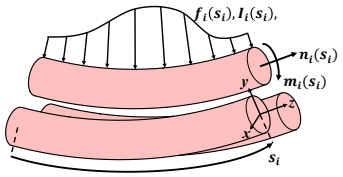

Figure 4. The distribution of internal and external forces and moments on the SRL.

To solve the postures of the parallel segment through integration, it is necessary to determine the boundary conditions. The boundary condition at the proximal end of the parallel segment serves as the initial value. In contrast, at the distal end, it is used for verifying the integration results.

The FRA and the connecting parts are combined in a fixed form, preventing relative motion. Consequently, the entire FRA can resist forces and moments from any direction, causing 6 unknowns about the internal forces and moments. Additionally, the length of the neutral axis after elongation is unknown. Therefore, there are 21 unknowns within a segment (3FRAs in total), serving as the proximal boundary condition.

According to the static equilibrium of the parallel segment, the relationship between the internal and external forces and moments at the distal end ($s_i = l_i$) is as follows:

$$\sum_{i=1}^{3}[n_i(l_i)] - F = 0$$

$$\sum_{i=1}^{3}[p_i(l_i) \times n_i(l_i) + m_i(l_i)] - p_d \times F - M = 0 \quad (7)$$

where F and M are external forces and moments applied on the center point of the parallel segment's distal end p_d, and R_d is the orientation of p_d. For each FRA within a parallel segment, the end of the neutral axis is in a specific positional relationship with p_d, and the orientation of the neutral axis at the distal end closely approximates R_d, expressed as follows:

$$p_d + R_d r_i - p_i = 0 \text{ for } i = 1 \dots 3$$

$$[log(R_i(l_i)^T R_d)]^\vee = 0 \text{ for } i = 1 \dots 3 \quad (8)$$

where r_i is a constant representing the distance between p_d and the FRA distal end. $log()$ represents the natural logarithm of a matrix, and $\vee$ is contrast with of $\wedge$. There are 6 constraints in (7) (the error of $n_i(l_i)$ and $m_i(l_i)$), and (8) demonstrate 6 constraints for each FRA (the error of $p_i(l_i)$ and $R_i(l_i)$), resulting in 24 constraints in total, thus allowing for the complete constraint of unknowns and the solving of the differential equation system.

C. Kinematic Model of the SRL

The SRL can be considered as a composition of three variable cross-section FRAs in parallel (combination of the FRAs in 3 segments). Thus, the kinematic model of the SRL differs from that of the parallel segment, requiring a segmented integration strategy. The FRAs in different segments have different dimensional parameters, leading to variations in properties such as K_{se} and K_{bt}. The solution of the kinematic model of the SRL begins from the proximal segment, which is similar to section B. However, the middle and distal segments use the integration results from the distal end of the previous segment as proximal boundary conditions which is indicated as: $n_{j,i}(0) = n_{j-1,i}(l_i)$, $m_{j,i}(0) = m_{j-1,i}(l_i)$ for $i = 1 \dots 3$ and $j = 2,3$. There are a total of 63 unknowns for the 9 FRAs including internal forces and moments, and the length of the FRA.

For the distal boundary conditions, the equality between internal forces and external loads at the distal end of the variable cross-section FRAs provides 6 constraints, and the constraints about positions and orientations provides 18 constraints, which have the same principles to (7) and (8).

Extra constraints about the SRL are required to integrate the posture. Using $j = 1,2,3$ to represent the index from the proximal segment to distal segment, and i as the FRAs order within a segment. The first condition is the balance of internal forces and moments at the at the connecting parts between segments in series:

$$\sum_{i=1}^{3} n_{j,i}(0) - n_{j-1,i}(l_i) = 0$$

$$\sum_{i=1}^{3} m_{j-1,i}(0) - m_{j,i}(l_i) = 0, \text{for } j = 2,3. \quad (9)$$

which provides 6 constraints in total. Additionally, for the FRAs in proximal and middle segment, there are still position and orientation constraints causing by connecting parts:

$$\left|p_{j,i}(l_i) - p_{j,k}(l_k)\right| = r_n, \left[log\left(R_{j,i}(l_i)^T R_{j,k}(l_k)\right)\right]^\vee = 0$$

$$\text{for } i = 1,2,3,\ j = 1,2,\ \ k = 2,3,1. \qquad (10)$$

where r_n represents the distance between the neutral axes of the FRAs in a segment. The distal end of the FRA in each segment maintains a fixed distance r_n and equal orientations. Thus, a total of 6 sets of equation systems are generated by the 2 parallel segments through (10), resulting in 36 constraints. By summarizing the above equations, a total of 72 constraints are obtained, so that the kinematic model of the SRL can be solved.

D. Algorithmic Approach of the Kinematic Model

To solve the kinematic model of the SRL, initial conditions about the starting point should be given first. The differential equations system is then solved based on the known conditions to obtain the corresponding results, then comparing with the constraints at the distal end. By adjusting the initial value through iteration step, the results will be gradually approached. Thus, as the first step, the 63 unknowns are combined into a vector uk as an initial value: $[n_{1x}(0)\ n_{1y}(0)\ n_{1z}(0)\ m_{1x}(0)\ m_{1y}(0)\ m_{1z}(0)\ l_1 \ldots]^T$.

Additionally, the residuals of (7) - (10) are combined as:

$$Res = \begin{bmatrix} \sum_{i=1}^{3} n_{3,i}(l_i) - F \\ \sum_{i=1}^{3} \left[m_{3,i}(l_i) + p_{3,i}(l_i) \times n_{3,i}(l_i)\right] \\ -p_d \times F - M \\ p_d + R_d r_i - p_{3,i} \\ \left[log\left(R_{3,i}(l_i)^T R_e R_{\alpha i}\right)\right]^{\vee} \\ \sum_{i=1}^{3} n_{j,i}(0) - n_{j-1,i}(l_i) \\ \sum_{i=1}^{3} m_{j-1,i}(0) - m_{j,i}(l_i) \\ \left|p_{j,i}(l_i) - p_{j,k}(l_k)\right| - r_n \\ \left[log\left(R_{j,i}(l_i)^T R_{j,k}(l_k)\right)\right]^{\vee} \end{bmatrix}$$

, which represents the residual error of the iteration step.

Algorithm 1 The SRL kinematics derivation process

Input: position $\boldsymbol{p_d}$ and orientation $\boldsymbol{R_d}$ of the SRL, initial guess $\boldsymbol{uk}$, Tolerance=1e-6, maximum iteration time=1e5
Output: result of 3FRAs' neutral axes coordinates

```
while do
  for i = 1 to 3 do
    using uk to integrate for the i-th variable cross-section FRA's posture through (4) - (6)
    Res is obtained through (7) - (10)
  end for
  if (Res < Tolerance) then
    output integration result as the SRL posture, break
  else
    if (iteration time > maximum iteration number)
      output the latest solution, break
    else
      calculate Jacobian matrix J about Red and uk
      using Levenberg-Marquardt algorithm to update initial guess:
        uk_{k+1} = uk_k + (J_k^T J_k + λI)^{-1} J_k^T Red_k
    end if
  end if
end while
calculating target pressure of FRAs through (1) - (3)
```

To solve the differential equations system of SRL, a shooting strategy is adopted to primarily focus on the residual vector Res, and computing the Jacobian matrix $J = \frac{\delta Res}{\delta uk}$ concerning the unknowns. Finally, through iteration, the Res will gradually approach to zero until it meets the specified tolerance range, leading to the solution [23]. To compute Res, initial values for the unknowns at $s_i = 0$ need to be provided. These guesses will be used to integrate from $s_i = 0$ to $s_i = l_i$, and the Levenberg-Marquardt algorithm is used to update the initial values continuously. The updating of the guess values is as: $uk_{k+1} = uk_k + (J_k^T J_k + \lambda I)^{-1} J_k^T Res_k$, where k is the iteration times. λ is a damping metrics for one step of the iteration to find a smaller residual. This process will continue in a loop until the tolerance range is met, as shown in Algorithm 1. Once the kinematic model solves for the current posture of the SRL, the coordinates of the neutral axis allow for the calculation of the length of each FRA, and the target pressure is gained through equation (1) - (3). This kinematic model calculates the static posture of the SRL at a given moment in time. The calculation process of a parallel segment is like that of the SRL, with Res removing (9), (10).

IV. CONTROL SYSTEM OF SRL

To accurately accomplish SRL's complex manipulations, a control system for SRL is designed and integrated with the kinematic model to achieve posture control of SRL. The control system of the SRL mainly consists of three parts: posture calculation, motion control, and motion data acquisition, as shown in Fig. 5.

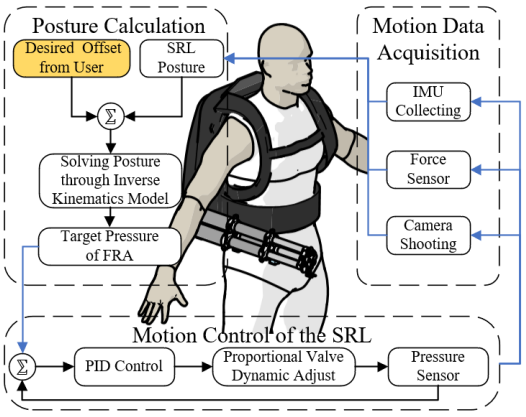

Figure 5. The control system of SRL.

During the posture calculation process, at regular intervals, the desired offset of the SRL's distal end, derived from the user's intent is obtained. This desired offset is then combined with the current posture data of the SRL, acquired from various sensors. Using the inverse kinematics model, the desired posture of the SRL at next intervals as well as the target pressure of each FRA are calculated. The process is mentioned in Algorithm 2. Finally, the target pressure of each FRA is transmitted to motion control system.

The motion control section uses a neural network PID strategy to gain the proportional, integral, and differential coefficients. The state model of PID controller is:

$$u_k = k_p e_k + k_i T \sum_{j=0}^{k} e_j + k_d (e_k - e_{k-1}) \qquad (11)$$

where $e_k = \kappa - \kappa_t$, κ is the current pressure and κ_t is the target pressure calculated by the analytic model, u_k is the output pressure. The k_p, k_i and k_d are proportional, integral, and differential coefficients. Transforming u_k into the expression of neural network PID strategy:

$$u_k = \sum_{i=1}^{3} \omega_{ik} x_{ik}$$

$$\omega_{ik} = \omega_{ik-1} + \eta e_k x_{ik} (\partial \kappa_{k+1} / \partial u_k) \qquad (12)$$

where ω_{ik} represents the weighting coefficients of x_{ik}, η represents the learning rate, and $\partial \kappa_{k+1} / \partial u_k$ represents the adjustment direction of the weighting coefficient. $x_{1k} = e_k$,$x_{2k} = T \sum_{j=0}^{k} e_j$,$x_{3k} = (e_k - e_{k-1})$ are input equations.

The control system is implemented through a microcontroller (Mega2560, Arduino). A micro air pump (KZP-PF, Kamoer) is used to provide stable air pressure to FRAs. The adjustment of air pressure is achieved through proportional valves (ITV1030-212L, SMC), and the detection of pressures upon FRAs are performed using pressure sensors (XGZP6857A, dspsence). The motion data acquisition section collects the position and orientation of the SRL using cameras (Realsence D435i, Intel) and IMUs (N100-Mini, wheeltec), which is then transmitted back to the computer. Besides, the force and moment applied on the distal end of the SRL is capture by the ATi-gamma six-axial force sensor.

V. Experiment

A. Motion Performance of the SRL's Prototype

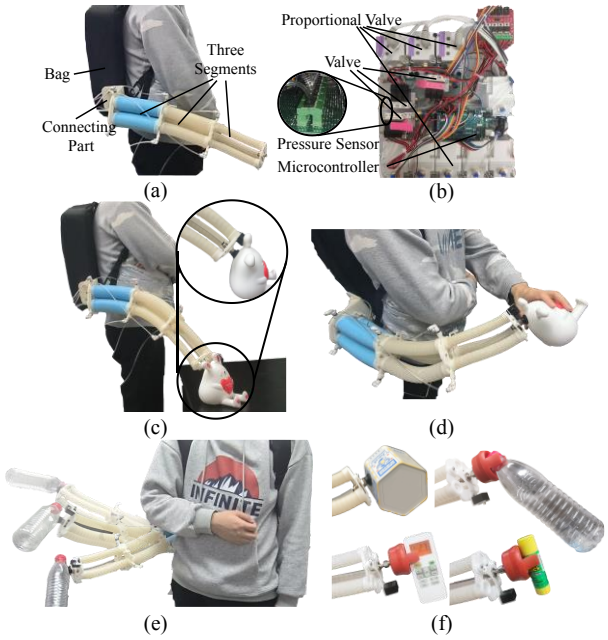

Figure 6. The prototype of SRL and motion performance. (a,) The construction of the SRL; (b) The structure of the control platform in the bag; (c) SRL adjusts its posture to approach the item, then uses the end effector to pick up the item; (d) SRL carries the item to a range accessible to the user; (e) SRL has high flexibility and a large workspace, capable of picking up items from different directions; (f) Combining with varying end effectors, SRL can effectively adapt to various items.

The prototype of the SRL and the control platform is shown in Fig. 6(a, b). The platform is integrated and placed inside the bag. The motion performance of the SRL is verified through experiments: The SRL starts from an initial static state and, by adjusting the internal pressure of the FRAs, continuously modifies its posture. The SRL carries the end effector along a trajectory calculated by the kinematic model to grasp the item outside the user's reachable range, as shown in Fig. 6(c). After completing the grasping action, the SRL changes its posture and transports the item to the position accessible to the user. Finally, it releases the object, thereby completing the task of assisting the user, as shown in Fig. 6(d), a vacuum suction cup is employed as the end effector to facilitate item grasping. A depth camera is used to recognize the user's 3D skeleton and obtain the coordinates of the user's hands. The SRL takes the user's hand coordinates as the endpoint of its movement to complete the delivery of objects.

The total weight of the SRL soft limb is 1.08 kg, and the payload of the SRL can reach 3.73 N. The SRL has a large workspace (0.52m×0.74m×0.66m), enabling user to adopt objects from different orientations, as shown in Fig. 6(e), effectively expanding the capabilities of users. SRL can adapt to various scenarios with the change of the end effector, as shown in Fig. 6(f).

B. Verification of the SRL Control Accuracy Performance

There are mainly two modes of motion for a parallel segment: elongation generated by equal air pressure applied to three FRAs and bending motion generated by different air pressures applied to three FRAs.

For the elongation experiment, pressure from 0 to 55kPa is applied to the FRA in proximal segment, and the corresponding elongation of the segment is recorded. Then, the kinematic and the finite element models are used to fit the corresponding elongation and record the pressure required for each FRA, the results are in Fig. 7(a, b).

For the bending motion, the focus is on the differences in the bending angles of the parallel segment. The bending experiment includes two experiments, the first applies 0 - 60 kPa pressure to two of the three FRAs in the proximal segment, while the remaining FRA is not pressurized, as shown in Fig. 7(c). In the second experiment, focusing on the middle segment, the three FRAs are pressurized separately from 0, reaching 20, 40, and 60 kPa, as shown in Fig. 7(e).

The Mean Absolute Error $(MAE(X,h) = \frac{1}{m}\sum_{i=1}^{m} |h(x_i) - y_i|$,where $h(x_i)$ and y_i are estimated values and actual values) is used to evaluate the error of the model. The result of the first bending experiment is shown in Fig. 7(d), and the second bending experiment set is shown in Fig. 7(f, g, h). The calculated results are shown in TABLE I. ,demonstrating that the kinematic model can accurately fit the parallel segment posture.

TABLE I. The Calculated MAE of Three Experiment

Motion type		Mean Absolute Error
Elongation		0.4440kPa
Bend1		0.7252kPa
Bend2	***20kPa***	0.8331kPa
	40kPa	0.6646 kPa
	60kPa	0.8300 kPa

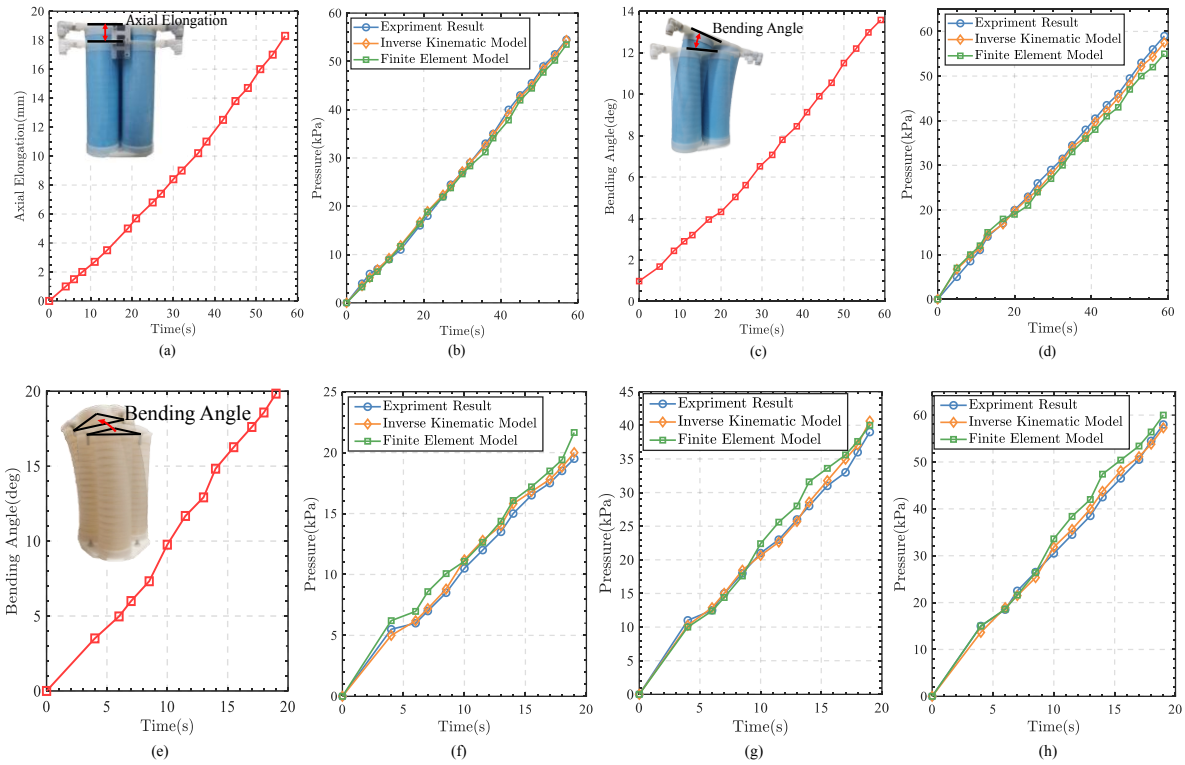

Figure 7. Verification of the accuracy of the kinematic Model of parallel segments. (a) The axial elongation of the proximal segment under elongation motion, the three FRAs are under pressure from 0 to 55kPa; (b) The results of two models fitting experiment result of elongation motion;(c) The bending angle of the proximal segment under bending motion, the two of three FRAs are under pressure from 0 to 60kPa;(d) The results of two models fitting experiment result of 60kPa under bending motion; (e) The bending angle of the middle segment under bending motion, with three FRAs under pressure from 0 to 20,40 and 60kPa; (f, g, h) The results of two models fitting experiment result of 20,40 and 60 kPa under bending motion.

To further evaluate the effectiveness of the kinematic model in estimating SRL postures, the SRL is under pressure to take on a complex posture: the FRAs in the proximal segment are pressurized at 90, 60, and 30 kPa; in the middle segment at 60, 40, and 20 kPa, and in the distal segment at 50 kPa equally. Eventually, by identifying the neutral axis of the SRL, the change trend of the posture curve of the SRL is obtained, and the kinematic and finite element models are fit the posture separately and obtain the corresponding posture curve, as shown in Fig. 8(a).

TABLE II. COMPARISON WITH CURRENT SOFT SRLS

	Workspace	Weight	Payload Capacity	Control Error
Proposed SRL	0.52×0.74×0.66m	1.08kg	3.73N	2.02%
Soft Poly-Limb [13]	0.55×0.69×0.72m	1.6kg	3.43N	4.69%
Fabric SPL [14]	0.63×0.69×0.28m	1.1kg	14.72N	3.90%
Soft flippers [12]	0.23m× 150°	0.46kg	113N	Not mention

The deformation results of the SRL experiment and the two models are shown in Fig. 8(b, c, d). The *R-square* ($R\text{-}square = 1 - \frac{\sum_{i=1}^{n}(\hat{y}_i - y_i)^2}{\sum_{i=1}^{n}(y_i - \bar{y})^2}$, where y_i and $\hat{y}_i$ are the actual value and calculated value, $\bar{y}$ denotes the mean of y_i) is used to represent the fit of the results. The *R-square* of the kinematic model is 0.882, while the finite element model is 0.869. Compared to the experiment results, the Euclidean displacement error at the end for the kinematic model is 13.45mm with an error of 2.02% to the whole length. For the finite element model, it is 17.96mm with an error of 2.43%. Therefore, the kinematic model demonstrates a good effect in capturing of the SRL posture.

Compared to the current representative soft SRL in TABLE II. , SRL proposed in this paper performs larger workspaces, lighter weight, and higher control accuracy. The load-bearing capacity of the SRL is primarily limited by the micro air pump. However, if the use of the SRL is restricted to a small range of indoor environments, an additional large air source can be employed to further enhance the load-bearing capacity of the SRL.

VI. CONCLUSION

In this paper, inspired by the octopus's arm, a soft SRL based on FRA is proposed. Furthermore, the kinematic model for the SRL is established, along with the control system to control the SRL posture precisely. Finally, the accuracy of the proposed kinematic model is verified through experiments, and the motion performance of SRL's prototype is carried out, exhibiting its flexibility and adaptability to various scenarios.

Future work will focus on developing human-robot interaction strategy, combining multiple sensory data to improve the efficiency of interaction. Additionally, advancing human-machine collaboration with the SRL

through sensor feedback [11] or using imitation learning methods [26] also holds significant research value. Besides, SRL can adapt to different application scenarios by varying its size and wear position. Therefore, it is necessary to construct a human-robot coupling model to achieve the optimal wearing experience.

REFERENCES

[1] M. A. Sada, M. Khamis, A. Kato, S. Sugano, et al. "Challenges and Opportunities of Supernumerary Robotic Limbs," CHI 2017 workshop on Amplification and Augmentation of Human Perception, 2017, pp. 123-135.

[2] F. Parietti, H. H. Asada, "Supernumerary robotic limbs for aircraft fuselage assembly: body stabilization and guidance by bracing." IEEE International Conference on Robotics and Automation, 2014, pp. 1176-1183, doi: 10.1109/ICRA.2014.6907002.

[3] D. A. Kurek and H. H. Asada, "The MantisBot: Design and impedance control of supernumerary robotic limbs for near-ground work," 2017 IEEE International Conference on Robotics and Automation (ICRA), Singapore, 2017, pp. 5942-5947, doi: 10.1109/ICRA.2017.7989700.

[4] J. Guggenheim, R. Hoffman, H. Song and H. H. Asada, "Leveraging the human operator in the design and control of supernumerary robotic limbs," IEEE Robotics and Automation Letters, vol. 5, no. 2, 2020, pp. 2177-2184, doi: 10.1109/LRA.2020.2970948.

[5] C. Khazoom, P. Caillouette, A. Girard, J. S. Plante, "A supernumerary robotic leg powered by magnetorheological actuators to assist human locomotion," IEEE Robotics and Automation Letters, 2022, pp. 5143-5150, doi: 10.1109/LRA.2020.3005629.

[6] C. Véronneau et al., "Multifunctional Remotely Actuated 3-DOF Supernumerary Robotic Arm Based on Magnetorheological Clutches and Hydrostatic Transmission Lines," in IEEE Robotics and Automation Letters, 2020, pp. 2546-2553, doi: 10.1109/LRA.2020.2967327.

[7] F. Parietti, K. C. Chan, B. Hunter, H. H. Asada, "Design and control of supernumerary robotic limbs for balance augmentation," IEEE International Conference of Robotics and Automation., 2015, pp. 5010–5017.

[8] P. Polygerinos, N. Correll, S. A. Morin, B. Mosadegh, C. D. Onal, K. Petersen, R. F. Shepherd, "Soft robotics: Review of fluid- driven intrinsically soft devices; manufacturing, sensing, control, and applications in human- robot interaction," Advanced Engineering Materials, 2017, pp. 1438-1656, doi = "10.1002/adem.201700016.

[9] G. Chen, T. Lin, L. Gabriel, A. Ji, "Design of an active flexible spine for wall climbing robot using pneumatic soft actuators," Journal of Bionic Engineering, 2023, pp.530-542, doi=10.1007/s42235-022-00273-2.

[10] P. Polygerinos, Z. Wang, K.C. Galloway, R. J. Wood, C. J. Walsh, "Soft robotic glove for combined assistance and at-home rehabilitation," Robotics and Autonomous Systems, 2015, pp. 135-143, doi: 10.1016/j.robot.2014.08.014.

[11] Guan, Q., Stella, F., Della Santina, C. et al. Trimmed helicoids: an architectured soft structure yielding soft robots with high precision, large workspace, and compliant interactions. npj Robotics (2023).

[12] S. Liu et al., "Otariidae-inspired soft-robotic supernumerary flippers by fabric kirigami and origami," in IEEE/ASME Transactions on Mechatronics, vol. 26, no. 5, pp. 2747-2757, Oct. 2021, doi: 10.1109/TMECH.2020.3045476.

[13] PH. Nguyen, C. Sparks, SG. Nuthi, NM. Vale, P. Polygerinos, "Soft poly-limbs: toward a new paradigm of mobile manipulation for daily living tasks," Soft Robotics, 2019, pp.38-53, doi:10.1089/soro.2018.0065.

[14] P. H. Nguyen, I. B. Imran Mohd, C. Sparks, F. L. Arellano, W. Zhang and P. Polygerinos, "Fabric Soft Poly-Limbs for Physical Assistance of Daily Living Tasks," 2019 International Conference on Robotics and Automation, 2019, pp. 8429-8435, doi: 10.1109/ICRA.2019.8794294.

[15] A. Ahmadi, M. Asgari, "Novel bio-inspired variable stiffness soft actuator via fiber-reinforced dielectric elastomer, inspired by Octopus bimaculoides," Intelligent Service Robotics, 2021, pp. 691-705, doi: 10.1007/s11370-021-00388-1.

[16] Kier W M, Stella M P. The arrangement and function of octopus arm musculature and connective tissue[J]. Journal of Morphology, 2007, 268(10): 831-843.

[17] L. Marechal, P. Balland, L. Lindenroth, et al. "Toward a common framework and database of materials for soft robotics," Soft Robotics, 2021, pp.284-297, doi: 10.1089/soro.2019.0115.

[18] F. Connolly, C. J. Walsh, K. Bertoldi, "Automatic design of fiber-reinforced soft actuators for trajectory matching," Proceedings of the National Academy of Sciences of the United States of America, 2017, pp. 51–56, doi:10.1073/pnas.1615140114.

[19] X. Xue, Z. Zhan, Y. Cai, L. Yao, Z. Lu, (2019). "Design and finite element analysis of fiber-reinforced soft pneumatic actuator," Intelligent Robotics and Applications, 2019, pp.641-651, doi:10.1007/978-3-030-27526-6_56.

[20] Y. Tian, Q. Zhang, D. Cai, C. Chen, J. Zhang, and W. Duan, "Theoretical modelling of soft robotic gripper with bioinspiredfibrillar adhesives," Mechanics of Advanced Materials and Structures, 2021, pp. 2250–2266, doi:10.1080/15376494.2020.1857482.

[21] M. Luc, B. Pascale, L. Lukas, P. Fotis, et al. "Toward a Common Framework and Database of Materials for Soft Robotics." Soft robotics," 2020, pp. 284-297, doi:10.1089/soro.2019.0115.

[22] M. Bartholdt, M. Wiese, M. Schappler, S. Spindeldreier and A. Raatz, "A parameter identification method for static Cosserat rod models: Application to soft material actuators with exteroceptive sensors," 2021 IEEE/RSJ International Conference on Intelligent Robots and Systems, Prague, Czech Republic, 2021, pp. 624-631, doi: 10.1109/IROS51168.2021.9636447.

[23] J. Till, C. E. Bryson, S. Chung, A. Orekhov and D. C. Rucker, "Efficient computation of multiple coupled cosserat rod models for real-time simulation and control of parallel continuum manipulators," 2015 IEEE International Conference on Robotics and Automation, Seattle, WA, USA, 2015, pp. 5067-5074, doi: 10.1109/ICRA.2015.7139904.

[24] G.A. Holzapfel, "Nonlinear solid mechanics: A continuum approach for engineering," Meccanica 37, 2002, pp:489–490, doi: 10.1023/A:1020843529530.

[25] Webster III, Robert J., and Bryan A. Jones. "Design and kinematic modeling of constant curvature continuum robots: A review." The International Journal of Robotics Research, 2010, pp: 1661-1683.

[26] A. Hussein, M. M. Gaber, E. Elyan, and C. Jayne, "Imitation learning: A survey of learning methods. ACM Computing Surveys (CSUR), 50(2), 2017, pp: 1-35. doi=10.1145/3054912.